RSC Advances

PAPER

View Article Online
View Journal | View Issue

Cite this: *RSC Adv.*, 2022, **12**, 35350

Solution processed high performance perovskite solar cells based on a silver nanowire-titanium dioxide hybrid top electrode†

Khalid Mahmood, ‡*[a] Hafiz Husnanin Akhtar,‡[a] Haji Ghulam Qutab,[a] Naveed Ramzan,[b] Rabia Sharif, [a] Abdul Rehman, [a] Arshi Khalid[c] and Muhammad Taqi Mehran[d]

Received 27th October 2022
Accepted 27th November 2022

DOI: 10.1039/d2ra06778a

rsc.li/rsc-advances

Longer silver nanowires (AgNWs) > 50 μm and even 90 μm in length have been produced *via* a polyol method by just changing the stirring speed at a temperature of 130 °C. As-synthesized longer AgNWs are further utilized to construct transparent conductive AgNWs films by a facile drop-casting technique that attained a sheet resistance of 14.5 Ω sq^{-1} and transmittance over 85%, which is higher than ITO film. The use of a AgNWs/TiO_2 hybrid electrode decreases the sheet resistance to 8.3 Ω sq^{-1}, which is attributed to the enhancement of connections between AgNWs by filling the empty spaces between nanowires and TiO_2 nanoparticles. Transparent perovskite solar cells (PSCs) on the basis of these AgNWs and AgNWs/TiO_2 hybrid top electrodes were made and examined. Due to the light scattering nature of TiO_2 nanoparticles, optical transmittance of the AgNWs/TiO_2 hybrid electrode enhances to some extent after the coating of a TiO_2 layer. Both cell efficiencies and stability of the PSCs are enhanced by using the AgNWs/TiO_2 top electrode. A power conversion efficiency (PCE) of 10.65% was attained for perovskite devices based on only the AgNW electrode with a sheet resistance of 14.5 Ω sq^{-1}. A PCE of 14.53% was achieved after coating with TiO_2 nanoparticles, indicating the layer effect of TiO_2 coating.

1. Introduction

Owing to their better performance, integration and consistency, transparent conducting oxides (TCOs) are the crucial components of future optoelectronic gadgets like touch screens, solar cells and liquid crystal displays.[1–5] A transparent conductive electrode (TCE) having decent mechanical flexibility is a crucial part of these devices. Over the past few years, indium tin oxide (ITO), was well recognized as a most suitable transparent conductor material due to its exceptional optical and electrical characteristics.[2,5–8] On the basis of its brittleness and high temperature processing conditions, ITO is being substituted with some other future generation transparent conductors namely metal nanowires, conducting polymers, graphene and carbon nanotubes.[9,10]

Among the metal nanowires, particularly silver nanowires (AgNWs) have gained the attraction of researchers owing to their greater conductivity, viable and economical film formation methods.[11–13] AgNW electrodes have attained a great optical transmittance over 90% and lower sheet resistance of 49 Ω sq^{-1}, depending on their nature and synthesis method. The composition, diameter and length of the AgNWs are the most important factors affecting the performance of nanowires based transparent electrode. The length and diameter of nanowires are the most crucial features which provide the better combination of electrical conductivity and optical transmittance but it is very tough to control them instantaneously. Scientists have suggested a number of approaches for producing nanostructures in past decade, largely separated into physical and techniques.[14–16] In recent years, polyol method has been established as the most promising route for synthesizing the AgNWs by just controlling the few process parameters such as stirring speed, growth temperature and time.[17,18] Hence, the quest for the economical and appropriate synthesis technique is of great interest these days that can simultaneously control the diameter and length of silver nanowires. We did a broad literature review and summarized the parameters that influence the structure of nanowires in the polyol method.[19] We established that, other than growth temperature, the stirring speed is also

[a]*Department of Chemical & Polymer Engineering, University of Engineering & Technology Lahore, Faisalabad Campus, 3½ Km. Khurrianwala – Makkuana By-Pass, Faisalabad, Pakistan. E-mail: khalid@uet.edu.pk*

[b]*Department of Chemical Engineering (ChE), University of Engineering & Technology (UET), Lahore, Pakistan*

[c]*Department of Humanities & Basic Sciences, University of Engineering & Technology Lahore, Faisalabad Campus, 3½ Km. Khurrianwala – Makkuana By-Pass, Faisalabad, Pakistan*

[d]*School of Chemical and Materials Engineering, National University of Sciences and Technology NUST, H-12, Islamabad, Pakistan*

† Electronic supplementary information (ESI) available. See DOI: https://doi.org/10.1039/d2ra06778a

‡ There authors contribute equally to this work.

very critical. Thus, a viable and direct polyol method is suggested here for the growth of extra-long AgNWs by merely tuning the stirring speed. Conclusively, the longer AgNWs will be useful to construct transparent conducting films using a simple drop-coating technique and measured the sheet resistance and transmittance of the corresponding films.

Perovskite solar cells (PSCs) have attained great consideration as a talented photovoltaic technology owing to their inexpensive nature, ease of processing and higher efficiencies.[20–22] In the recent past, semitransparent PSCs have been extensively developed for their specific use in solar windows, rooftops and perovskite/CIGS tandem devices, where the characteristics of top electrode govern the overall effectiveness of solar devices.[23,24] It is important that solution-based electrodes should be established for building of PSCs. Among numerous suggested transparent electrodes, AgNWs transparent electrode has low sheet resistance and high transparency at 550 nm.[25] The utilization of AgNWs as top/bottom transparent electrodes have established in the recent past,[26–28] and proven to be the most talented solution-processed electrodes in PSCs.[29–31] Nevertheless, due to the nature of perovskite crystal and unsuitability between the electrode and the other interface layers, stalled development of solution-processed electrodes in PSCs, which results in lower power conversion efficiency (PCE) of 8–13% as reported previously.

Here, using balanced interface engineering together with proper choice of solution-processes film formation practices, we establish the low-temperature treating of AgNWs as top electrodes for highly effective and stable semitransparent PSCs. For the first time ever, we formed a hybrid electrode consisting of AgNWs/TiO_2 which helps in physical interaction permitting the solution-formation of th AgNWs and guarantees ohmic connection connecting the PC60BM ([6,6]-phenyl C61-butyric acid methyl ester) and nanowires in a better way. The results show that sheet resistance of the AgNWs/TiO_2 hybrid electrode reduced meaningfully by refining the interconnection of AgNWs.[32] Owing to the exceptional match of the AgNWs/TiO_2 hybrid electrode with the beneath interface layers, the fabricated devices displayed complete open-circuit voltage (Voc) and high fill factors (FFs) with promising device efficiency. With the help of this tactic, PCE of the semitransparent PSCs improved from 10.65% to 14.53%.

2. Experimental details

2.1 Materials

Silver nitrate ($AgNO_3$), iron chloride ($FeCl_3$), polyvinylpyrrolidone (PVP) and ethylene glycol (EG), $TiCl_4$, NH_4OH, ethanol and acetone comprising of analytical grades were brought and used as such without any modification. $PbCl_2$ and CH_3NH_3I were properly mixed having mole ratio of 1 : 3 and poured in dimethyl formamide with a concentration of 30%. Afterwards, mixture was thoroughly stirred for 3 h at 60 °C. PC60BM was melted in chlorobenzene having a concentration of 20 mg mL^{-1} and agitated at 60 °C for 3 h prior to use.

2.2 Hydrolysis procedure for the synthesis of TiO_2 nanoparticles

Chemical precipitation technique was used to form TiO_2 nanoparticles. TiO_2 nanoparticles were produced by hydrolyzing $TiCl_4$ in a reaction environment with glycerol. In a typical procedure, 18.96 g of 9.11 M $TiCl_4$ was poured dropwise to the solution comprising of glycerol and water using an ice-bath under strong stirring. After the reaction was completed, 300 mL of 2.5 M NH_4OH was poured dropwise to the solution till the pH approaches 10. At that stage, white precipitates of TiO_2 were produced. Later, the liquid phase was drawing off from the solid part. Now, the subsequent precipitates were centrifuge at 4000 rpm for 10 min by drying them overnight at 80 °C. Then, the TiO_2 powder was calcined at 400 °C for 1 h, creating off-white powder.

2.3 Synthesis of AgNWs and hybrid of AgNWs/TiO_2 by polyol method

In a typical polyol synthesis process, for the first solution 0.2 g of PVP having molecular weight of 360 000 (g mol^{-1}) was poured into 25 mL of EG and fully melted *via* magnetic stirring under ambient conditions, where PVP shows the role of surfactant while preparation of nanowires. In terms of growth process, a mutual approach is that PVP interacts intensely with Ag atoms on the facets that act as a structure-defining agent also the capping agent stopping accumulation. Chain length of PVP imparts a significant part in defining the yields and dimensions of AgNWs. After that, 0.25 g of silver $AgNO_3$ was poured into as-prepared PVP solution and stirred continuously until obtained a uniform and transparent solution. Secondly, 3.5 g of $FeCl_3$ solution (600 μM in EG) was made and poured into the first solution. The combined mixture was then directly shifted to a preheated reactor (130 °C) for the grow AgNWs for a reaction time of 5 h. Subsequently, centrifugation was done at 4000 rpm for 5 min and the residue was thoroughly washed with acetone and ethanol. Finally, as-synthesized AgNWs were completely distributed in ethanol for their further usage as transparent electrode. Hybrid of AgNWs/TiO_2 was synthesis by adding the well mixed solution of TiO_2 (in ethanol) into the finally dispersed nanowires in ethanol. Drop-coating technique was finally used to construct thin films of nanowires onto the glass substrates and drying under ambient atmosphere.

2.4 Fabrication of perovskite devices

The fluorine-doped tin oxide (FTO) glass substrates were carefully washed using isopropanol and acetone *via* ultrasonic bath. A thin layer of PEDOT:PSS was made using doctor blading at 50 °C and heated at 140 °C for 10 min before transferring the substrates into the nitrogen filled glove box. Then, perovskite precursor was spin-coated for 45 s and 2000 rpm followed by heating at 110 °C for 40 min. PC60BM precursor was then deposited over the $CH_3NH_3PbI_3$-xCl_x perovskite film *via* spin-coating at 1000 rpm for 45 s. Lastly, AgNWs layer was spin casted above of it. For the devices with AgNWs/TiO_2 hybrid

electrode, the layer was also prepared using spin-coater using the above prepared solution.

2.5 Films characterization and property measurements

Morphology investigation of the nanowires was conducted *via* scanning electron microscope (SEM, SU1510, Hitachi, Japan). The development of the Ag stage was verified using an X-ray diffraction (XRD) analysis (Model M18XHF). Sheet resistance and optical transmittance of the films were obtained with the help of four-point probe and an UV-VISNIR spectrometer (Lambda 950, from Perkin), respectively. The current density–voltage (*J–V*) curves of the perovskite cells were obtained with a Keithley 2400 source meter with a simulated sun AM 1.5 G. The external quantum efficiency (EQE) spectra were verified using EQE evaluation system (QE-R) and the light intensity was standardized using a standard single crystal Si photovoltaic cell.

3. Results and discussion

3.1 XRD analysis of AgNWs

The formation of silver phase was investigated by X-ray diffraction (XRD) analysis. Fig. 1 displays comparison of XRD configurations of synthesized AgNWs and commercially available AgNWs, which specifies that nanowires made by solution technique are decently in the face-centred cube (fcc) phase. The high intensity peaks located at angles of $2\theta = 38.1°$, 44.2°, 64.3°, and 77.5° match the (111), (200), (220), and (311) crystal planes, respectively, which is accordance to (JCPDS 65-2871). The XRD shape discloses that AgNWs production using polyol method contain pure phase. This directed the successful development of the crystalline AgNWs. The intensity ratio between (111) and (200) mounts demonstrates a comparatively high number of 3.3 related to the hypothetical value of 2.5, which shows the improvement of crystal-like planes in the {111} AgNWs.

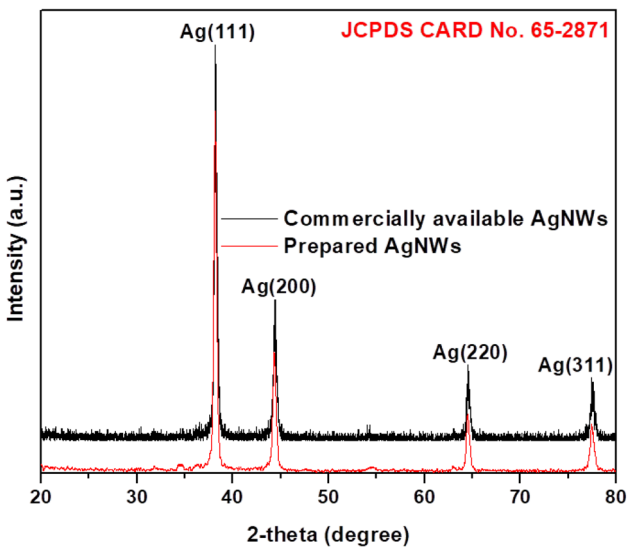

Fig. 1 Comparison of XRD patterns of prepared AgNWs and commercially available AgNWs.

3.2 SEM analysis of AgNWs

The morphological investigation of AgNWs was studied using SEM images. Firstly, the stirring speed was controlled to study its influence on AgNWs formation as revealed in Fig. 2 at 130 °C. It is clearly realized that the wires formation and length essentially relies on the stirring speed. It is observed that (Fig. 2(a)) shorter wires together with huge aggregates of unequal shaped nanoparticles are formed at very high stirring speed of 600 rpm. Though, a much lower speed of 300 rpm formed longer nanowires with lesser nanoparticles (Fig. 2(b)).

Besides, at 0 rpm, without shaking the precursor formed pure very-long AgNWs and no nanoparticles (Fig. 2(c)). Without agitation, nanowires length significantly increased to above 70 μm, even few nanowires have longer enough to show length of 100 μm. Hence, by merely controlling the mechanical movement, the formation of long AgNWs *via* viable polyol procedure has been attained, which concludes that a special environment comprising of no interference is needed for the growth of longer and clear nanowires. It reveals that a static precursor state with sufficient crystal growth period and a low growth temperature of 130 °C are essentially needed for the smooth formation of nanowires during the nucleation stage. It is obvious that AgNWs have almost identical diameters, *i.e.*, the diameter is not dependent on agitation. The governing diameter is around 60 nm with a minor variation of further diameters. The percentage of wires comprising of 60 nm diameter was above 90% without agitation. No obvious changes in the diameter by changing stirring speed direct that the nucleation and development of Ag were leading reasons in directing the diameter of nanowires in the polyol method.

Low magnification SEM image of longer nanowire is shown in Fig. 3(a), demonstrates the complete coverage of AgNWs over the entire surface of glass substrate and the yield of silver product is over 95% using polyol method. High resolution SEM image (Fig. 3(b)) is also displays to clearly see the nanowires interconnection.

To identify the effect of growth temperature on the development of nanowires, AgNWs have also been produced at 110 and 170 °C without agitation (0 rpm) as shown in SEM images (Fig. 3). At much low temperature of 110 °C, longer reaction time of 10 h is required for the complete and slower formation of AgNWs, which is elongated time period compared to nanowires growth at 130 °C. Most of the nanowires had length above 60 μm; in reality few wires are longer than 120 μm (Fig. 4(a)). On the other hand, wires were successfully grown in just 40 min, at much higher reaction temperature of 170 °C. But, the wires are of shorter length only 20–30 μm (Fig. 4(b)), along with the nanoparticles growth. These findings support the fact that very long AgNWs could be preferably grown at lower reaction temperature and longer time correspond using a simple and viable polyol method.

3.3 Optical transmittance and sheet resistance measurements of AgNWs

A simple drop-casting technique was used to make transparent conductive films of AgNWs synthesized at optimum process

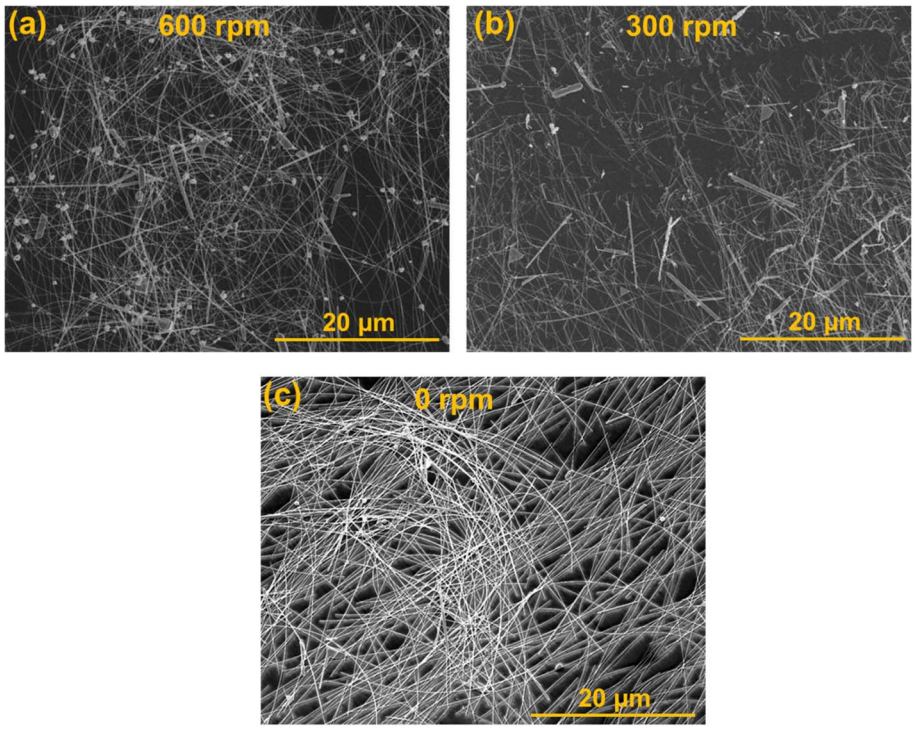

Fig. 2 SEM images (a–c) showing the influence of stirring speed on the growth of AgNWs.

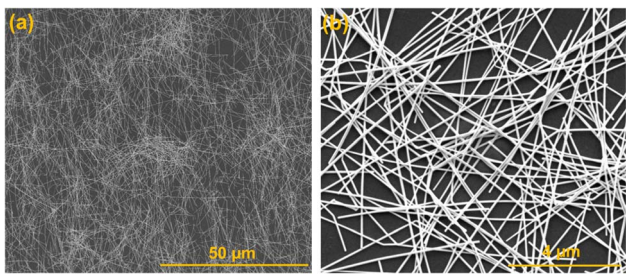

Fig. 3 SEM images (a and b) of long AgNWs showing better surface coverage and interconnectivity between nanowires.

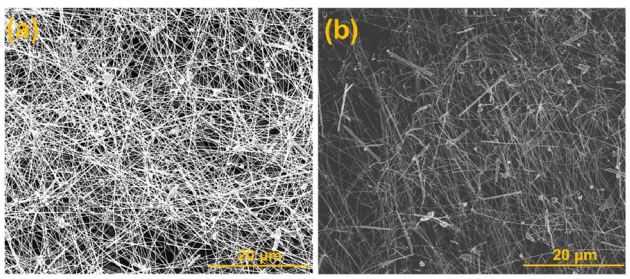

Fig. 4 SEM images (a and b) presenting the consequence of growth temperature on the formation of AgNWs.

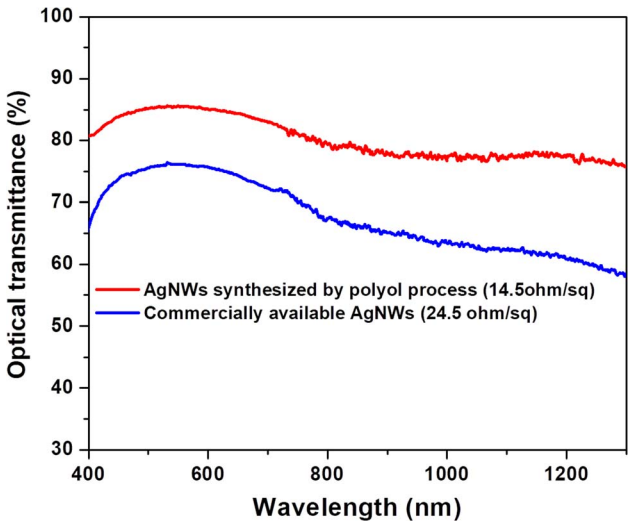

Fig. 5 Evaluation of transmittance spectra and sheet resistance of AgNWs synthesized by polyol method and commercially available nanowires.

conditions (130 °C and 0 rpm). Fig. 5 displays the comparison of transmittance and sheet resistances of AgNWs films synthesized by polyol process and commercially available AgNWs. The optical transmittance mainly influenced by the quantity of AgNWs over the substrate surface.

In case of commercially available nanowires the sheet resistance and optical transmittance were 24.5 Ω sq^{-1} and 75%, respectively. Besides, using AgNWs prepared by polyol process, the corresponding values were 14.5 Ω sq^{-1} and 87%, correspondingly. Clearly a low confrontation of 14.5 Ω sq^{-1} and better optical transmittance has been attained for the long

AgNWs. The obtained numbers are also better than conventionally available ITO film. The reason behind the better results is the formation of longer nanowires by a simple polyol method which create a random web within the contacts of nanowires, which avoids the undesired contact resistance in transparent conductive layers per unit area in comparison with related shorter naowires.

3.4 Transmittance and sheet resistance measurements of AgNW/TiO_2 hybrid films

In order to further increase the functionality of the AgNWs networks transparent films, TiO_2 added to the Ag nanowires dispersed in ethanol to coat the surface of nanowires with TiO_2 nanoparticles. Fig. 6 exhibits the assessment of sheet resistance and optical transmission spectra of the AgNW/TiO_2 hybrid film with only AgNWs transparent conductive film. As realized here clearly, AgNWs/TiO_2 hybrid films demonstrate the outstanding performance in term of high optical transmittance and better conductivity (low sheet resistance of 8.3 Ω sq^{-1}) compared to only AgNWs films. The slight increase in light transparency is credited to the light scattering result of TiO_2 nanoparticles over the nanowires surface. Besides, low sheet resistance of AgNWs/TiO_2 hybrid electrode was due to the better interconnectivity between AgNWs webs and TiO_2 nanoparticles.

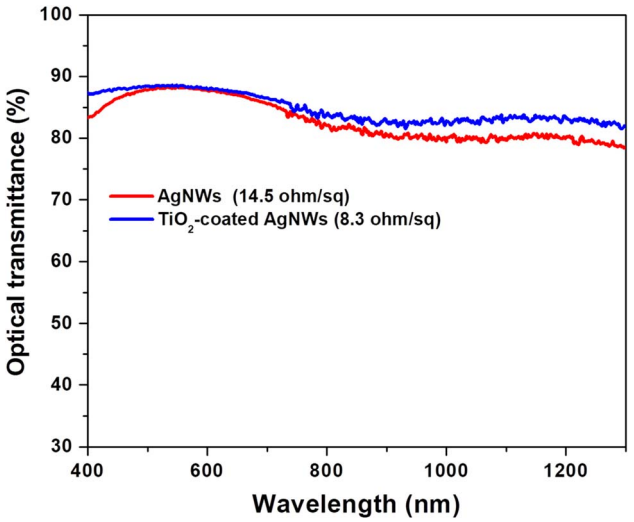

Fig. 6 Evaluation of transmittance spectra and sheet resistance of AgNWs and AgNWs/TiO_2 hybrid electrode.

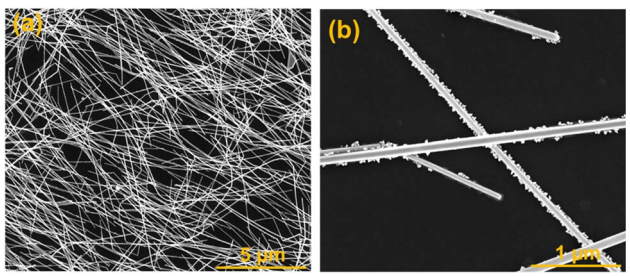

Fig. 7 SEM images (a and b) of TiO_2-coated AgNWs.

3.5 SEM analysis of TiO_2-coated AgNWs

In order to realize the reason for the reduction in sheet resistance of the AgNWs transparent conductive films after coating TiO_2 nanoparticles, SEM analysis was further utilized to investigate the surface nanostructure of AgNWs/TiO_2 hybrid films. As shown in Fig. 7, TiO_2 nanoparticles are evenly coated onto the surface of AgNWs and voids between the nanowires are typically filled with TiO_2 nanoparticles which ensures better conductivity and enhanced optical transmittance.

3.6 Perovskite devices with AgNWs and AgNWs/TiO_2 hybrid electrodes

A planar-heterojunction solar cell construction was selected in the current study owing to ease of fabrication, low-cost materials and high performance. Fig. 8(a) displays the schematic illustration of complete device with a layer order of Glass/ITO/PEDOT:PSS/perovskite/PC60BM/AgNWs and Glass/ITO/PEDOT:PSS/perovskite/PC60BM/AgNWs/TiO_2. The perovskite absorber layer is inserted between the PC60BM and PEDOT:PSS that helps as an electron and a hole hindering film, respectively. Fig. S1† displays the cross-sectional SEM image of fabricated whole device, which reveals a well-established layer structure. In Fig. 8(b), we show the transmittance spectra of the complete cell with and without AgNWs/TiO_2 top electrode. It is observed that the fabricated semitransparent device having ~140 nm-thick perovskite absorber layer reveals an average visible

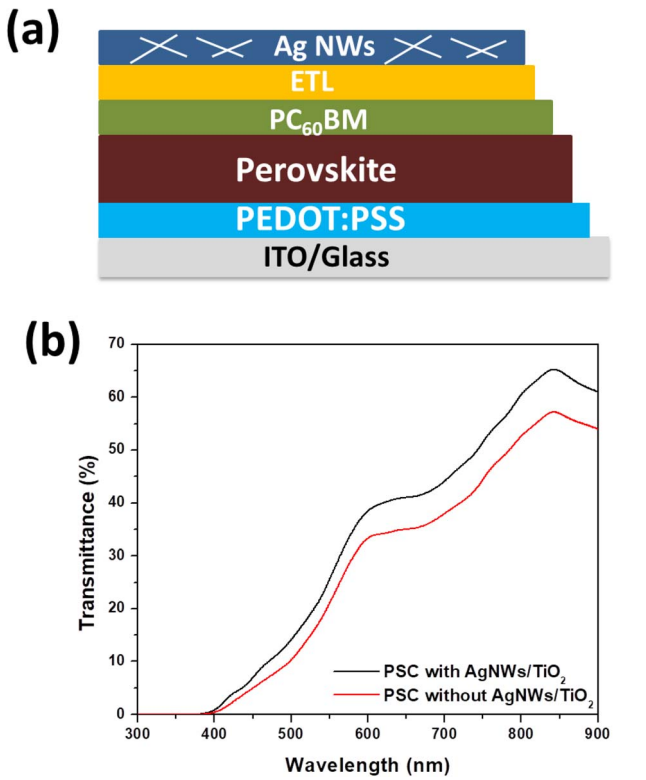

Fig. 8 (a) Simplified illustration of the PSCs having AgNWs on top, and (b) transmittance spectra of the device without and with AgNWs/TiO_2 as top electrode.

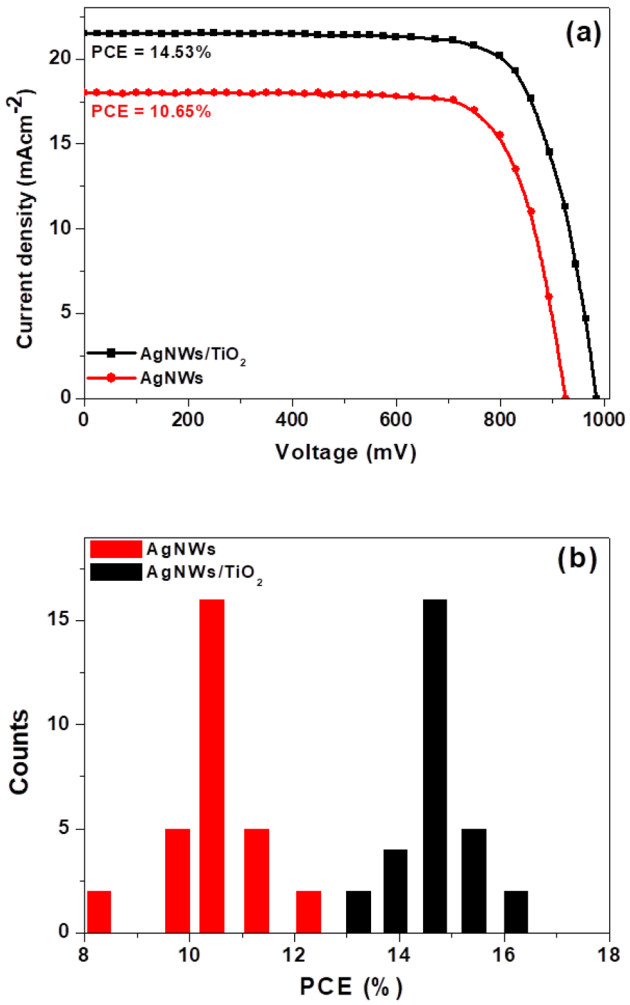

Fig. 9 (a) *J–V* curves of the perovskite devices having AgNWs and AgNWs/TiO_2 hybrid electrodes and (b) histogram of PCE of 30 individual devices based on same electrodes.

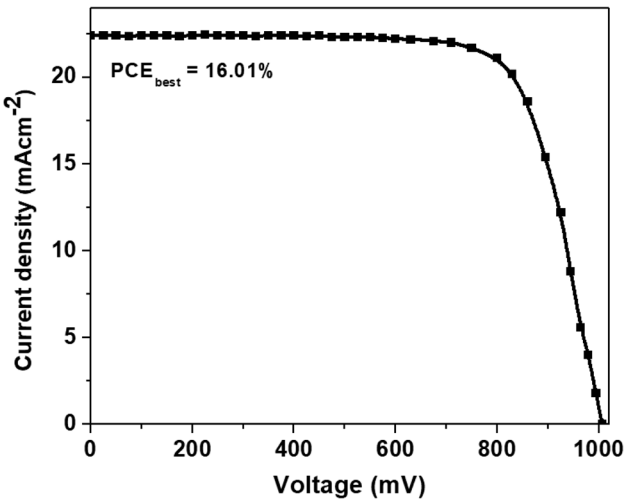

Fig. 10 *J–V* plot of the most efficient perovskite device with AgNWs/TiO_2 hybrid electrode.

transparency (AVT) of 28.1%, that is comparable to the value stated by Roldán-Carmona.[33] Fig. 9(a) displays the *J–V* plots of the perovskite devices fabricated with AgNWs and AgNWs/TiO_2 hybrid top electrodes and the corresponding photovoltaic data is summarized in Table 1. It can be realized clearly, the devices with pristine AgNWs electrode presented a power conversion efficiency (PCE) of 10.65% with a current-density (J_{SC}) of 18 mA cm^{-2}, open-circuit-voltage (V_{oc}) of 925 V and a fill factor (FF) of 64%. In order to further promote the efficiency of the AgNWs based devices, surface of nanowires was also decorated with TiO_2 nanoparticles to form AgNWs/TiO_2 hybrid electrode. After decorating with TiO_2 nanoparticles, devices showed significantly enhanced PCE of 14.53%, which is much better than previously reported efficiency data for cells based on AgNWs/ZnO hybrid top electrodes.[29,31] As discussed above, AgNWs/TiO_2 hybrid electrode reveal the exceptional performance in term of high optical transmittance and better conductivity (low sheet resistance of 8.3 Ω sq^{-1}) compared to only AgNWs films. It shows that decreasing the nanowires sheet resistance is also advantageous for enhancing the device efficiency by decreasing the series resistance of the perovskite solar cells. In other words, coating of TiO_2 nanoparticles over AgNWs certainly increases device performance due to the better interconnection between AgNWs networks with TiO_2 nanoparticles. The improved cell efficiency may be due to many other factors, not necessarily a better interconnection between the nanowires and the nanoparticles. For example, the electrode thickness, length and diameter of the nanowires, distribution of the nanoparticles on the hybrid (homogeneity), type of interfaces and interaction between them, and between the new electrode an the previous solar cell layer, and other features. In addition, the semiconductor TiO_2 nanoparticles increase the surface and the interfaces that the hybrid material has which favors photons absorption and impairs transparency. To confirm the precision of the measured current density, we did external quantum efficiency (EQE) analysis. As presented in Fig S2.† the device with AgNWs/TiO_2 hybrid electrode obviously show a high EQE value of 76% at 550 nm, compared to those based on only AgNWs. Based on the EQE data, the J_{SC} values can be calculated theoretically to be 17.3 and, 20.9 mA cm^{-2} for AgNWs and AgNWs/TiO_2 based devices, respectively. The error between the integrated value (from EQE) and J_{SC} values measured from *J–V* curves is less than 5%. The ultraviolet-visible absorption spectra

Table 1 Device parameters for perovskite devices with AgNWs and AgNWs/TiO_2 hybrid electrodes

Electrode type	J_{SC} (mA cm^{-2})	V_{OC} (mV)	FF (%)	PCE (%)	PCE_{max} (%)
AgNWs	18.0	925	64	10.65	12.47
AgNWs/TiO_2	21.5	980	69	14.53	16.01

of the perovskite absorber are presented in Fig. S3 (ESI†). Moreover, PCE variation was establish to be closer for the solar cells after coating with TiO_2 nanoparticles (Fig. 9(b)). The closet PCE variation of the AgNWs/TiO_2 hybrid electrode was credited to enhanced consistency after the coating of TiO_2 nanoparticles, as established by low sheet resistance for the AgNWs/TiO_2 electrode.

The *J–V* plot of the most efficient perovskite solar cell based on AgNWs/TiO_2 hybrid electrode is presented in Fig. 10. These cells produced the best power conversion efficiency (PCE_{best}) of 16.01%, the first and highest PCE ever stated for perovskite devices based on AgNWs/TiO_2 hybrid electrode to date.

4. Conclusion

AgNWs larger than 70 μm and somehow 110 μm in length are manufactured *via* a low-temperature (130 °C) and solution-processed polyol method by regulating the growth temperature and stirring speed. No agitation of reaction mixture and longer reaction time are preferable for the better growth of nanowires without the formation any undesired particles those eventually affect the desire performance of wires. The wires length is above three times lengthier compared to the commercially available AgNWs and comparable to ITO. Due to smooth nucleation growth, length distribution of wires is quite narrow compared to other methods. Transparent electrodes have been constructed using these log AgNWs, that attained a sheet resistance of 14.5 Ω sq^{-1} with 87% transmittance under ambient condition, even the measured numbers are far better than ITO films. Efficiency of these AgNWs based transparent electrodes was further improved by coating a thin layer of TiO_2 nanoparticles over the nanowires surface by simply mixing a TiO_2 precursor in the well dispersed nanowires. The performance improvement of AgNWs/TiO_2 hybrid electrode is associated with the better interconnectivity between the nanowires after managing the empty spaces in nanowires by coating TiO_2 nanoparticles. We also evidently proved that AgNWs/TiO_2 hybrid electrode can assist as top electrode of perovskite solar cells. Device efficiency rises by covering the surface of AgNWs with TiO_2 nanoparticles, which was attributed to the fall of sheet resistance of the AgNWs electrode. A remarkable PCE of 16.01% has been achieved for the perovskite with AgNWs/TiO_2 hybrid electrode.

Conflicts of interest

There are no conflicts to declare.

Acknowledgements

The authors gratefully acknowledge the financial support from the Higher Education Commission (HEC) of Pakistan.

References

1 X. Liu, D. D. Li, X. Chen, W. Y. Lai and W. Huang, *ACS Appl. Mater. Interfaces*, 2018, **10**, 32536–32542.
2 Y. Li, Y. Li, Z. Fan, H. Yang, X. Yuana and C. Wang, *RSC Adv.*, 2020, **10**, 21369–21374.
3 R. Manda, S. Pagidi, Y. J. Lim, R. He, S. M. Song, J. H. Lee, G. D. Lee and S. H. Lee, *J. Mol. Liq.*, 2019, 111314.
4 C. Yumi, S. K. Chang and J. Sungjin, *Materials*, 2018, **11**, 2231.
5 J. Jiu, M. Nogi, T. Sugahara, T. Tokuno, T. Araki, N. Komoda, K. Suganuma, H. Uchida and K. Shinozaki, *J. Mater. Chem.*, 2012, **22**, 23561.
6 T. Tokuno, M. Nogi, J. Jiu and K. Suganuma, *Nanoscale Res. Lett.*, 2012, **7**, 281.
7 M. Ye, X. Hong, F. Zhang and X. Liu, *J. Mater. Chem. A*, 2016, **4**, 6755–6771.
8 C. Prabukumar and K. U. Bhat, *Mater. Today: Proc.*, 2018, **5**, 22487–22493.
9 J. Y. Lee, S. T. Connor, Y. Cui and P. Peumans, *Nano Lett.*, 2008, **8**, 689.
10 R. Zhu, C. Chung, K. Cha, W. Yang, Y. Zheng, H. Zhou, T. Song, C. Chen, P. Wei, G. Li and Y. Yang, *ACS Nano*, 2011, **5**, 9877.
11 S. Wang, Y. H. Tian, C. X. Wang, C. J. Hang, Y. L. Huang and C. Liao, *Compos. Sci. Technol.*, 2019, **174**, 76–83.
12 C. Yumi, S. K. Chang and J. Sungjin, *Materials*, 2018, **11**, 2231.
13 T. Lei, R. X. Peng, W. Song, L. Hong, J. M. Huang, N. N. Fei and Z. Y. Ge, *J. Mater. Chem. A*, 2019, **7**, 3737–3744.
14 H. Kim, Y. Park, D. Choi, W. S. Chu, S. H. Ahn, D. M. Chun and C. S. Lee, *Appl. Surf. Sci.*, 2018, **456**, 19–24.
15 H. W. Sheng, X. T. Zhang, Y. L. Ma, P. X. Wang, J. Y. Zhou, Q. Su, W. Lan, E. Q. Xie and C. F. J. Zhang, *ACS Appl. Mater. Interfaces*, 2019, **11**, 8992–9001.
16 E. Lee, J. Ahn, H. C. Kwon, S. Ma, K. Kim, S. Yun and J. Moon, *Adv. Energy Mater.*, 2018, **8**, 1702182.
17 J. Jiu, K. Murai, D. Kim, K. Kim and K. Suganuma, *Mater. Chem, Phys.*, 2009, **114**, 333.
18 J. Jiu, M. Nogi, T. Sugahara, T. Tokuno, T. Araki, N. Komoda, K. Suganuma, H. Uchida and K. Shinozaki, *J. Mater. Chem.*, 2012, **22**, 23561.
19 Y. Sun, Y. Yin, B. Mayer, T. Herricks and Y. Xia, *Chem. Mater.*, 2006, **14**, 4736.
20 K. Mahmood, S. Sarwar and M. T. Mehran, *RSC Adv.*, 2017, **7**, 17044–17062.
21 K. Mahmood, A. Khalid, S. W. Ahmad, H. G. Qutab, M. Hameed and R. Sharif, *Sol. Energy*, 2021, **203**, 32–36.
22 K. Mahmood, M. Alzaid, A. Khalid, R. A. Malik, H. G. Qutab, S. W. Ahmad, A. Maqbool, F. Alsalh and N. Almoisheer, *Surf. Coat. Tech.*, 2021, **416**, 127160.
23 C. D. Bailie, M. G. Christoforo, J. P. Mailoa, A. R. Bowring, E. L. Unger, W. H. Nguyen, J. Burschka, N. Pellet, J. Z. Lee, M. Gratzel, R. Noufi, T. Buonassisi, A. Salleo and M. D. McGehee, *Energy Environ. Sci.*, 2015, **8**, 956–963.
24 L. Kranz, A. Abate, T. Feurer, F. Fu, E. Avancini, J. Lockinger, P. Reinhard, S. M. Zakeeruddin, M. Gratzel, S. Buecheler and A. N. Tiwari, *J. Phys. Chem. Lett.*, 2015, **6**, 2676–2681.
25 J. Y. Lee, S. T. Connor, Y. Cui and P. Peumans, *Nano Lett.*, 2008, **8**, 689–692.

26 D. Langley, G. Giusti, C. Mayousse, C. Celle, D. Bellet and J. P. Simonato, *Nanotechnology*, 2013, **24**, 452001.
27 S. R. Ye, A. R. Rathmell, Z. F. Chen, I. E. Stewart and B. J. Wiley, *Adv. Mater.*, 2014, **26**, 6670–6687.
28 A. Kim, Y. Won, K. Woo, S. Jeong and J. Moon, *Adv. Funct. Mater.*, 2014, **24**, 2462–2471.
29 F. Guo, H. Azimi, Y. Hou, T. Przybilla, M. Y. Hu, C. Bronnbauer, S. Langner, E. Spiecker, K. Forberich and C. J. Brabec, *Nanoscale*, 2015, **7**, 1642–1649.
30 M. Lee, Y. Ko, B. K. Min and Y. Jun, *ChemSusChem*, 2016, **9**, 31–35.
31 K. Han, M. Xie, L. Zhang, L. Yan, J. Wei, G. Ji, Q. Luo, J. Lin, Y. Hao and C. Q. Ma, *Sol. Energy Mater. Sol. Cells*, 2018, **185**, 399–405.
32 R. Zhu, C. H. Chung, K. C. Cha, W. B. Yang, Y. B. Zheng, H. P. Zhou, T. B. Song, C. C. Chen, P. S. Weiss, G. Li and Y. Yang, *ACS Nano*, 2011, **5**, 9877–9882.
33 C. Roldán-Carmona, O. Malinkiewicz, R. Betancur, G. Longo, C. Momblona, O. Malinkiewicz, R. Betancur, G. Longo and C. Momblona, *Energy Environ. Sci.*, 2014, **7**, 2968–2973.